NASA TECHNICAL NOTE

NASA TN D-4312

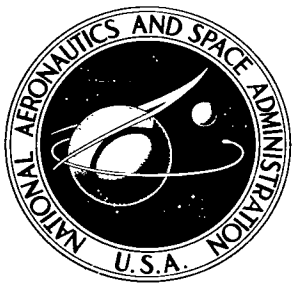




# PHOTOMETRY OF AN IRON ARTIFICIAL METEOR REENTERING AT 11 KILOMETERS PER SECOND

*by J. B. Robertson and Wendell G. Ayers*

*Langley Research Center*
*Langley Station, Hampton, Va.*

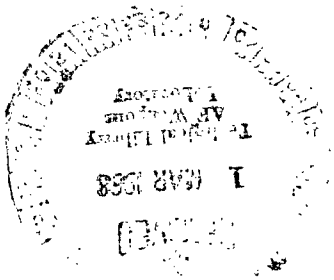

NATIONAL AERONAUTICS AND SPACE ADMINISTRATION • WASHINGTON, D. C. • FEBRUARY 1968

NASA TN D-4312

# PHOTOMETRY OF AN IRON ARTIFICIAL METEOR REENTERING AT 11 KILOMETERS PER SECOND

By J. B. Robertson and Wendell G. Ayers

Langley Research Center
Langley Station, Hampton, Va.

NATIONAL AERONAUTICS AND SPACE ADMINISTRATION

For sale by the Clearinghouse for Federal Scientific and Technical Information
Springfield, Virginia 22151 – CFSTI price $3.00

# PHOTOMETRY OF AN IRON ARTIFICIAL METEOR REENTERING AT 11 KILOMETERS PER SECOND

By J. B. Robertson and Wendell G. Ayers
Langley Research Center

## SUMMARY

A man-made meteor was successfully produced in March of 1966 by reentering into the atmosphere a 5.7-gram steel pellet at 10.85 km/sec with a six-stage, solid-fuel Trailblazer II vehicle, the last stage of which was an explosive accelerator. The meteor was photographed with a system of cameras and spectrographs. The luminous power of the meteor as a function of time was determined from the photographs with stars for calibration. The velocity and deceleration of the meteor were determined from photographs taken by cameras with chopping shutters. The luminous efficiency of the meteor was calculated from the luminous power and velocity data. The panchromatic luminous efficiency was $(4.0 \pm 0.8) \times 10^{-3}$ and the blue sensitive luminous efficiency was $(2.1 \pm 0.4) \times 10^{-3}$. A spectrogram of the meteor on blue sensitive film showed that the radiation produced by the meteor in the spectral region from 3800 Å to 5000 Å was predominately line radiation from neutral iron. A filter photograph indicated considerable radiation in the spectral region from 4900 Å to 6500 Å. A large portion of this radiation may have been produced by iron oxide.

## INTRODUCTION

One of the hazards encountered by spacecraft in their journeys outside the earth atmosphere is that of meteoroids. In order for design engineers to protect against this hazard, the magnitude of the hazard must be known. The magnitude of the meteoroid hazard is defined by a statistical knowledge of the number, mass, density, and energy of the meteoroids. One method of obtaining the statistical data is ground-based observation of the meteors which are produced when the meteoroids enter the earth atmosphere. Scientists have long been able to determine from photographs, the velocity, deceleration, trajectory, and luminous intensity of natural meteors. However, they could only estimate the mass of the meteoroid with an uncertainty far too large to adequately define the meteoroid hazard. It is the primary objective of the Meteor Simulation Project of the Langley Research Center to determine experimentally the values of the luminous efficiency of artificial meteors. This knowledge would allow a more accurate calculation of the mass

of the irradiating materials in natural meteors from photographs. The study of artificial meteors also provides a qualitative insight into some of the physical and chemical processes associated with very high-speed reentries into the earth atmosphere.

This paper presents the results of a flight experiment in which an artificial meteor was produced and the event recorded by ground-based cameras and spectrographs. Also reported is the luminous efficiency of the meteor calculated from the photographic data. The luminous efficiency of a meteor is the efficiency with which a meteor converts its kinetic energy into luminous energy.

## SYMBOLS

| | |
|---|---|
| $H$ | effective irradiance, ergs per centimeter$^2$-second |
| $H_o$ | effective irradiance of a zero-magnitude meteor, ergs per centimeter$^2$-second |
| $H_\lambda$ | spectral irradiance, ergs per centimeter$^2$-second-angstrom |
| $M$ | magnitude |
| $m$ | mass, grams |
| $m_i$ | initial mass of meteor, grams |
| $P$ | luminous power, ergs per second |
| $P_o$ | luminous power of a zero-magnitude meteor, ergs per second |
| $S_\lambda$ | spectral response |
| $t$ | time, seconds |
| $V$ | velocity, centimeters per second |
| $\lambda$ | wavelength, angstroms |
| $\tau$ | luminous efficiency |
| $\tau_o$ | luminosity coefficient, seconds per centimeter |
| $\tau_o'$ | luminosity coefficient, second$^4$ per gram-centimeter$^3$ |

Subscripts:

b blue sensitive, 3800 to 5000 angstroms

p panchromatic, 3800 to 7000 angstroms

r red, 5000 to 6400 angstroms

## DESCRIPTION OF EXPERIMENT

### Vehicle and Trajectory

The vehicle used in the experiment was a six-stage, solid-fuel Trailblazer II vehicle (fig. 1). A detailed description of the Trailblazer II vehicle can be found in reference 1. The first two stages boosted the velocity package to an altitude of approximately 300 km. The velocity package (fig. 2) contains the third, fourth, fifth, and sixth stages. After the velocity package passes apogee, the last four stages fire in rapid succession, driving the pellet into the earth atmosphere at meteor velocity. The vehicle trajectory is shown in figure 3.

The sixth and final stage of the system is an explosive accelerator. This accelerator gives the final and largest velocity increase to the pellet. The sixth-stage accelerator and the payload (reentry pellet) are varied from flight to flight in the meteor simulation series.

### Gun and Pellet

A diagram of the explosive accelerator (an air cavity gun) used in this experiment is shown in figure 4 and a description is given in reference 2. The pellet material was 1020 steel, which is more than 99 percent iron. A 7-gram disk of the material was held in place in front of the pentolite charge by a lucite ring. The explosion formed the steel into a cup-shaped pellet weighing about 5.7 grams plus several small fragments (fig. 5).

A series of ground tests were performed by Ballistics Research Laboratory to determine the mass, shape, and velocity of the pellet formed by this type of accelerator. The ground test pellets were captured in a target of low-density plastic and sawdust. Weighing of the captured pellets from five ground firings gave a pellet mass of $5.66 \pm 0.05$ grams. The pellet shape was determined from in-flight radiographs and from captured pellets (fig. 5). The velocity was determined by two-station radiography; measurements during seven ground tests gave $4.3 \pm 0.09$ km/sec.

## Instrumentation

The primary method of obtaining data is photography. More than 30 cameras located at four ground stations along the Virginia-North Carolina coast (fig. 6) were used in this experiment. These included modified K-24, modified K-37, BC-4, and Super Schmidt cameras. Blue sensitive and panchromatic photographic emulsions were used. Some of the cameras were equipped with chopping shutters and some were equipped with spectral gratings, prisms, or filters. The cameras were aimed at the expected reentry area. The shutters were opened 80 sec before expected reentry event time and closed 100 sec after the event.

Ground-based radars located at NASA Wallops Station tracked the first five stages of the vehicle from launch to give vehicle performance and trajectory data.

## Meteor Event

Trailblazer II-1 was launched from the NASA Wallops Station at 20:15:00 EST on the night of March 17, 1966. The steel pellet reentered into the atmosphere 383.7 sec after launch and produced a meteor (visible streak) in the sky off the coast of North Carolina. The beginning of the visible reentry occurred at an altitude of 70 km. At this altitude, the ratio of the molecular mean free path $\lambda$ to the characteristic body diameter $l$ was 0.033, which is in the slip-flow regime. The meteor was seen by observers and recorded by cameras at all four camera sites. The empty Cygnus 5, Cygnus 15, and X-248 rocket motor cases reentered after the meteor with enough velocity to produce visible streaks which were also recorded by cameras. Figure 7 is one of the photographs of the reentries.

# DATA REDUCTION

## Ballistics

The ballistic data of the meteor are obtained from the photographs by the method detailed in reference 3. The position and direction of the meteor were determined by using photographs from two stations. The velocity and deceleration data are calculated from photographs with chopped meteor trails made by cameras with repeating shutters. The velocity and deceleration of the meteor as calculated from three selected photographs are shown in figures 8 and 9. The initial velocity was calculated to be $10.85 \pm 0.05$ km/sec.

## Luminous Efficiency

The primary end product of this experiment is a value of the luminous efficiency $\tau$ of the meteor which can be defined by the equation

$$P = -\frac{1}{2}\tau\frac{dm}{dt}V^2 \tag{1}$$

where

$P$ luminous power radiated by meteor

$\frac{dm}{dt}$ rate of mass loss

$V$ velocity of meteor

The quantity $\frac{1}{2}\frac{dm}{dt}V^2$ is therefore the rate of loss of kinetic energy of the meteor due to ablation. Verniani (ref. 4) has determined from observational data that, for natural meteors, $\tau$ is proportional to the first power of the velocity. This leads to the definition of the luminosity coefficient $\tau_o$ by the equation

$$\tau_o = \frac{\tau}{V} \tag{2}$$

where $\tau_o$ is regarded as a constant. The luminous power $P$ is related to magnitude $M$ by

$$P = P_o \times 10^{-0.4M} \tag{3}$$

where $P_o$ is the luminous power of a zero-magnitude meteor.

The values of $\tau_o$ reported here were calculated from the values of $M$ and $V$ obtained from photographs and by using the equation

$$\tau_o = \frac{2P_o}{m_i}\int_{t_1}^{t_2} 10^{-0.4M(t)}V^{-3}(t)\,dt \tag{4}$$

where the time interval $t_1$ to $t_2$ is the duration of the meteor. The values $P_{o,b} = 5.0 \times 10^9$ ergs/sec and $P_{o,p} = 7.96 \times 10^9$ ergs/sec from reference 5, and the initial pellet mass $m_i = 5.66$ grams were used in equation (4). Data concerning the photographs selected for evaluation are given in table I.

The method used to calculate $\tau_o$ from the photographic data is given in references 5 and 6. In this method, points along the meteor trail are assigned magnitudes by comparing the photographic density of the meteor trail to photographic density of trails of stars of known magnitude which appear on the same photographic plate.

There are many factors that must be accounted for in determining the absolute magnitude of the meteor. Corrections were made for the difference in writing speeds of the

meteor and the stars, the difference in zenith angle, reciprocity failure of the film, and normalizing the meteor range to 100 km. The method normally used compares the peak densities of the meteor and star trails. In some photographs, the density profile of the meteor trail is different from that of the stars due to pellet fragmentation or optical aberrations. In these photographs, comparing peak densities would not yield the correct value for the magnitude of the meteor, and it is necessary to integrate under the exposure cross-section curve of the trails. This method was necessary for the analysis of one of the photographs used in this report.

### Errors

Some of the fragments created with the pellet by the explosive accelerator create small meteors of their own. These meteors are much dimmer and are shorter in length than the meteor of the main pellet. A few of these "debris" meteors were apparent in the photographs alongside the beginning of the main meteor.

The light energy of the debris meteors which are apparent in the photographs is not included in the sum of the pellet meteor energy because the images are spatially separated. However, if a debris meteor occurred in the plane defined by the camera and the pellet meteor, its image would be superimposed upon the image of the pellet meteor and its light energy would be included in the sum of the pellet meteor energy.

The largest of the debris meteors that can be identified for its entire length produced light energy equal to about 2 percent of the light energy of the pellet meteor. Had the image of this debris meteor been superimposed upon the image of the pellet meteor, the calculated value of $\tau_0$ would be high by approximately 2 percent.

The total error in $\tau_0$ results from errors in the values of mass, velocity, and magnitude. The errors in mass and velocity are statistical and are determined from repeated tests or repeated measurements. The probable error in magnitude is estimated and is a result of errors in film density measurements, star calibration curve, range calculation, and reciprocity failure correction. The probable errors in mass and velocity and their effect on $\tau_0$ are small compared to the size and effect of the probable error in meteor magnitude. The probable error in $M$ is estimated to be $\pm 0.2$ magnitude and causes a probable error in $\tau_0$ of $\pm 20$ percent.

## RESULTS AND DISCUSSION

### Broadband Data

The magnitude of the meteor as a function of time was measured from three photographs. The results are plotted in figure 10. The peak magnitude of the meteor was $M_b = -1.5$ and $M_p = -1.75$.

The resulting values of luminosity coefficient are

$$\tau_{o,b} = (1.9 \pm 0.4) \times 10^{-9} \text{ sec/cm}$$

$$\tau_{o,p} = (3.7 \pm 0.7) \times 10^{-9} \text{ sec/cm}$$

and

$$\tau'_{o,b} \equiv \frac{\tau_{o,b}}{P_{o,b}} = (3.9 \pm 0.8) \times 10^{-19} \text{ sec}^4/\text{gm-cm}^3$$

$$\tau'_{o,p} \equiv \frac{\tau_{o,p}}{P_{o,p}} = (4.7 \pm 0.9) \times 10^{-19} \text{ sec}^4/\text{gm-cm}^3$$

Using the initial velocity of 10.85 km/sec in equation (2) gives the luminous efficiencies of

$$\tau_b = (2.1 \pm 0.4) \times 10^{-3}$$

and

$$\tau_p = (4.0 \pm 0.8) \times 10^{-3}$$

The values of $\tau_o$ obtained in this experiment are compared, in table II, with those of other experiments (refs. 5, 7, and 8) to show the difference in values obtained from different meteors or different detector systems. Previously reported values of $\tau_o$ do not contain a correction for film reciprocity failure; therefore, the correction has been removed from the values of $\tau_o$ of this report in order to make the comparison. The reported value of $\tau_{o,p}$ agrees within a factor of 2 with previously reported values of $\tau_{o,p}$, and $\tau_{o,b}$ agrees within a factor of 2.5 with previous values of $\tau_{o,b}$.

## Spectral Data

The knowledge of the wavelength distribution of the light energy from artificial meteors offers some insight into the physical processes of the meteor event and sometimes leads to an understanding of differences in photometric data obtained with different camera systems.

The optical radiation from a meteor can be spectrally dispersed on the photographic emulsion by placing a suitable prism or grating before the lens of a camera; however, this can only be done at the sacrifice of the sensitivity of the photographic system. A limited amount of information can be obtained about the spectral distribution of the optical

radiation by the use of different photographic emulsion and optical filter combinations. Prisms and filters were used in this experiment to obtain information about the spectral distribution of the radiation from the artificial meteor.

Only one spectrogram of the meteor was obtained. This spectrogram was made with a Super Schmidt meteor camera (f/0.65) equipped with a six-element mosaic objective prism and blue sensitive (single-coated X-ray) photographic film. This system had an effective spectral sensitivity range from approximately 3700 Å to 5200 Å. The camera was operated by Smithsonian Astrophysical Observatory (SAO) personnel and was located at Sandbridge, Va.

A positive transparency of the original spectrogram was furnished to Langley by SAO and was compared with a spectrogram of another artificial meteor (ref. 9) for the purpose of wavelength identification. The comparison spectrum was obtained from a solid iron meteoroid which had an initial mass of 0.6 gram and a reentry velocity of 9.5 km/sec. The optical system used to obtain the comparison spectrum consisted of a grating and camera lens of fused silica (quartz) and X-ray photographic emulsion. The system had an effective spectral sensitivity range of approximately 3400 Å to 5200 Å. Microphotometer traces of the two spectrograms are presented in figure 11. The gross detail of the two spectra are essentially the same. The major radiation in both spectra is identified as atomic radiation from neutral iron.

Since the only spectrogram of this meteor was obtained on blue sensitive emulsion, that spectrogram gave no information about the radiation at wavelengths longer than 5000 Å. The spectra of earlier iron artificial meteors (ref. 7) display a considerable amount of radiation at wavelengths longer than 5000 Å which is identified as a mixture of line radiation from iron and band radiation from iron oxide.

A comparison of the amount of meteor radiation in the spectral band from 3700 Å to 5200 Å to the amount of radiation in the spectral band from 4900 Å to 6400 Å was obtained by photographing the artificial meteor with a camera equipped with a blue sensitive emulsion (Kodak Type 103-O) and a camera equipped with a panchromatic emulsion (Kodak Royal X) and a yellow filter (Kodak Wratten Filter No. 12). The two photographic detection systems are designated herein as blue and red, respectively.

Relative response curves for the two photographic detection systems are shown in figure 12(a). A spectrogram of an artificial meteor of iron dust (ref. 9) is included in figure 12(b) to show the radiation from an iron meteor that each system would record. The radiation in the spectrogram in figure 12(b) in the 3700 Å to 5000 Å band is very similar to the radiation in the spectrograms in figure 11 recorded on blue sensitive emulsions. The radiation beyond 4900 Å in the comparison spectrogram is a mixture of line radiation from neutral iron and band radiation from iron oxide (ref. 9). Since no dispersive elements were used with the two cameras, they produced photographs of the artificial

meteor having no spectral resolution within their bands of sensitivity. However, the optical densities of the images that were produced were a function of a weighted average of the radiation contained in the bandwidth of sensitivity.

The method of analysis used to make the comparison of the results of the two systems is as follows.

For a particular detection system, the effective irradiance $H$ is usually defined as

$$H = \int_0^\infty S_\lambda H_\lambda \, d\lambda \tag{5}$$

where $S_\lambda$ is the relative spectral response function of the system including the optical transmittance of the intervening media between the source and receiver and $H_\lambda$ is the spectral irradiance at the receiver through a lossless media.

A magnitude scale is then defined by the relationship

$$M = -2.5 \log \frac{H}{H_o} \tag{6}$$

The outputs from the two detection systems were compared by constructing an optical density versus magnitude scale for each system. Stars of color class A0 were used for this purpose. Values for optical density were obtained by measurement of the star images on the photographic plates. The values for stellar magnitude were obtained from standard catalogs and adjusted for the star position on the photographic plate. If the magnitudes of A0 stars are set equal for each system, then the ratio of the effective irradiance as determined by the blue system to the effective irradiance as determined by the red system is related to the magnitude scales by the equation

$$\frac{H_b}{H_r} = \frac{H_{o,b}}{H_{o,r}} 10^{0.4(M_r - M_b)} \tag{7}$$

The ratio $\frac{H_{o,b}}{H_{o,r}}$ was evaluated by using the spectral irradiance of the A0 star $\alpha$ Lyra from reference 10 (p. 83); this gives a value of

$$\frac{H_{o,b}}{H_{o,r}} = 1.4$$

The meteor magnitudes as measured by the red and blue systems are plotted as a function of time in figure 13. Magnitude values were calculated only at the indicated data points. A more detailed light curve (dashed line) from figure 10 is included for comparison. The radiation from the meteor consists primarily of iron line radiation in the blue

portion of the spectrum and is assumed to be a mixture of iron line radiation and iron oxide band radiation in the red portion of the spectrum. A reddening of the trail would occur if the iron oxide radiation increased at a greater rate along the trail than the iron radiation.

## CONCLUDING REMARKS

The initial reentry velocity of the pellet was determined to be 10.85 ± 0.05 km/sec. The meteor which was produced had a peak magnitude of $M_b = -1.5$ and $M_p = -1.75$. The luminosity coefficients and luminous efficiency of the meteor as calculated from the data are (for 10.85 km/sec)

$$\tau_{o,b} = (1.9 \pm 0.4) \times 10^{-9} \text{ sec/cm}$$

$$\tau_{o,p} = (3.7 \pm 0.7) \times 10^{-9} \text{ sec/cm}$$

$$\tau'_{o,b} = (3.9 \pm 0.8) \times 10^{-19} \text{ sec}^4/\text{gm-cm}^3$$

$$\tau'_{o,p} = (4.7 \pm 0.9) \times 10^{-19} \text{ sec}^4/\text{gm-cm}^3$$

$$\tau_b = (2.1 \pm 0.4) \times 10^{-3}$$

$$\tau_p = (4.0 \pm 0.8) \times 10^{-3}$$

where $\tau_o$ and $\tau'_o$ are luminosity coefficients and $\tau$ is the luminous efficiency, and the subscripts b and p refer to blue sensitive and panchromatic, respectively. A spectrogram of the meteor showed iron line radiation in the blue portion of the spectrum. The two-color photometry showed an increase in the ratio of the intensity of red light to the intensity of blue light along the trail. This change may have been caused by iron oxide radiation increasing at a greater rate along the trail than the iron radiation.

Langley Research Center,
National Aeronautics and Space Administration,
Langley Station, Hampton, Va., July 19, 1967,
709-06-00-01-23.

## REFERENCES


1. Lundstrom, Reginald R.; Henning, Allen B.; and Hook, W. Ray: Description and Performance of Three Trailblazer II Reentry Research Vehicles. NASA TN D-1866, 1964.

2. Kineke, John H., Jr.; and West, Carroll E., Jr.: An Improved Air-Cavity Explosive Charge for Accelerating Steel and Nickel Pellets. Mem. Rept. No. 1783, Ballistic Res. Labs., Aberdeen Proving Ground, Jan. 1967.

3. Whipple, Fred L.; and Jacchia, Luigi G.: Reduction Methods for Photographic Meteor Trails. Smithsonian Contrib. Astrophys., vol. 1, no. 2, 1957, pp. 183-206.

4. Verniani, Franco: Meteor Masses and Luminosity. Spec. Rept. No. 219 (NASA Grant NSR-09-015-033), Smithsonian Inst. Astrophys. Obs., Aug. 26, 1966.

5. Ayers, Wendell G.: Luminous Efficiency of an Artificial Meteor at 11.9 Kilometers Per Second. NASA TN D-2931, 1965.

6. Jacchia, Luigi G.: Photographic Meteor Phenomena and Theory. Tech. Rept. No. Three (Contracts NOrd 8555 and 10455), Harvard Coll. Obs. and Center Analysis, Massachusetts Inst. Technol., 1949.

7. Jewell, W. O.; and Wineman, A. R.: Preliminary Analysis of a Simulated Meteor Reentry at 9.8 Kilometers Per Second. NASA TN D-2268, 1964.

8. McCrosky, Richard E.; and Soberman, Robert K.: Results From an Artificial Iron Meteoroid at 10 km/sec. AFCRL-62-803, U.S. Air Force, July 1962.

9. Harvey, Gale A.: Photometry of Spectrograms of Three Artificial Meteors. NASA TN D-3930, 1967.

10. Code, A. D.: Stellar Energy Distribution. Stellar Atmospheres, Jesse L. Greenstein, ed., Univ. of Chicago Press, c.1960, pp. 50-87.

TABLE I.- DATA ON PHOTOGRAPHS SELECTED FOR EVALUATION

| Location | Camera | Focal length | f-number | Emulsion | Detector bandwidth | Spectral classification |
|---|---|---|---|---|---|---|
| Sandbridge, Va. | BC-4 | 304 mm | f/2.6 | Blue sensitive | 3800 Å to 5000 Å | b |
| Sandbridge, Va. | BC-4 | 304 mm | f/2.6 | Panchromatic | 3800 Å to 6400 Å | p |
| Coquina Beach, N.C. | K-24 | 178 mm | f/2.5 | Extended red | 3800 Å to 7000 Å | p |

TABLE II.- VALUES OF LUMINOSITY COEFFICIENT

| Source | Material | Mass, g | Velocity, km/sec | $\tau_{0,p}$, sec/cm | $\tau_{0,b}$, sec/cm | Comments |
|---|---|---|---|---|---|---|
| Robertson and Ayers (present report) | 1020 steel | 5.7 | 10.8 | $6 \times 10^{-9}$ | $1.7 \times 10^{-9}$ | Reciprocity failure correction removed |
| Unpublished data from SAO | 1020 steel | 5.7 | 10.8 | | $3.2 \times 10^{-9}$ | Same experiment as present report |
| Ayers (ref. 5) | Stainless steel | 2.2 | 11.9 | $10 \times 10^{-9}$ | | |
| Jewell and Wineman (ref. 7) | Stainless steel | 2.2 | 9.8 | [a]$7 \times 10^{-9}$ | | Color index removed from reported value |
| McCrosky and Soberman (ref. 8) | Stainless steel | 2.2 | 9.8 | | $4 \times 10^{-9}$ | Same experiment as ref. 7 |

[a]Reference 7 reports a value of $1.02 \times 10^{-9}$ for the visual luminous efficiency factor and states that the value was obtained from panchromatic data by applying a "color" correction of 1.65 magnitudes to the panchromatic data. Removal of the "color" correction gives the value for $\tau_{0,p}$ shown here.

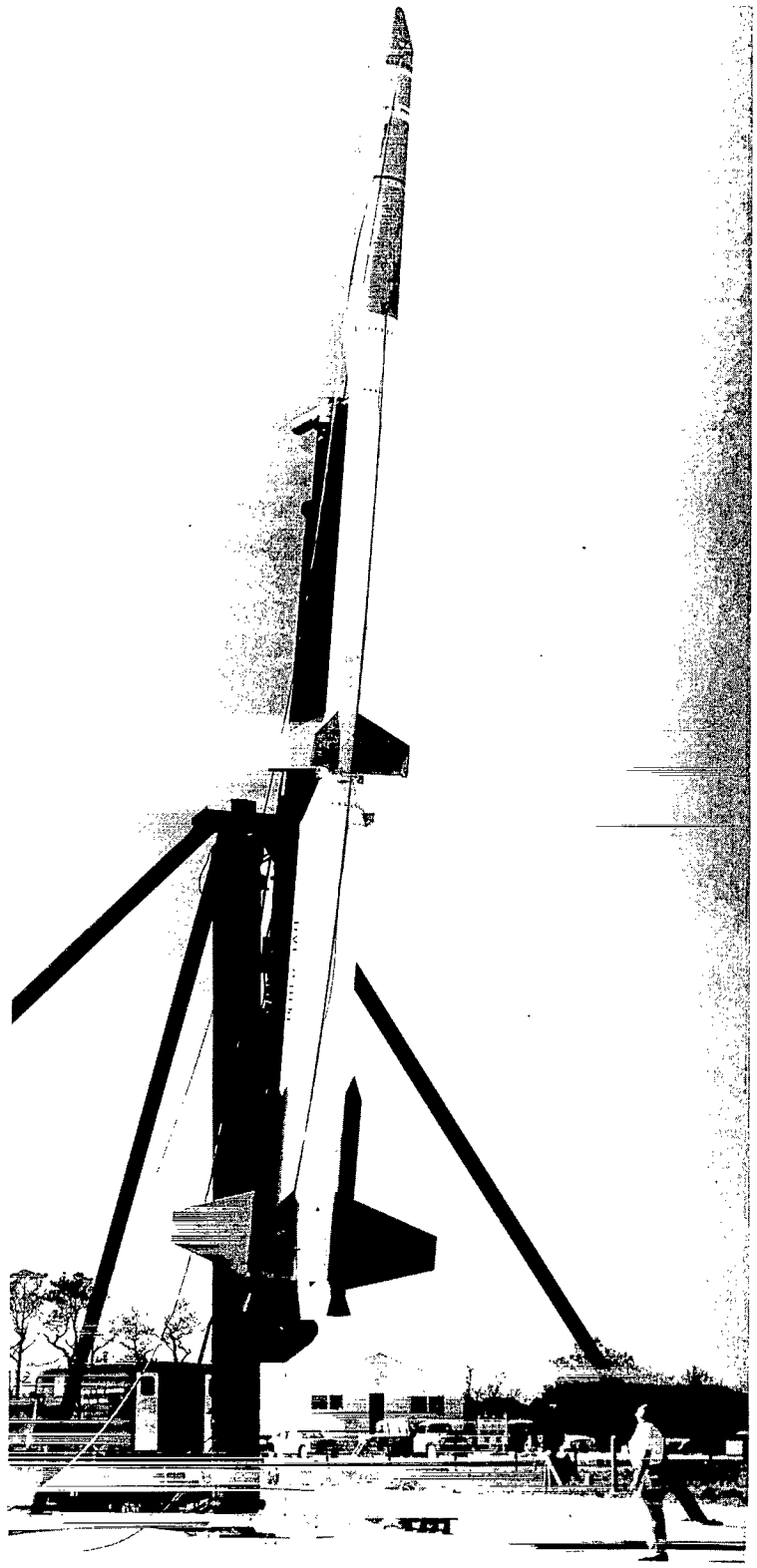

Figure 1.- Trailblazer II vehicle in launch position. L-62-4432

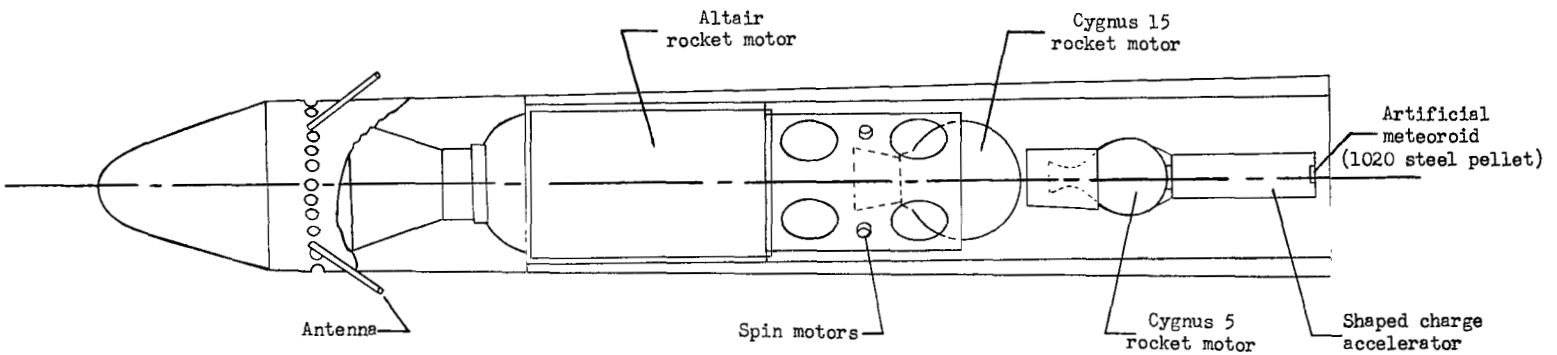


Figure 2.- Velocity package of Trailblazer II vehicle with artificial meteor payload.

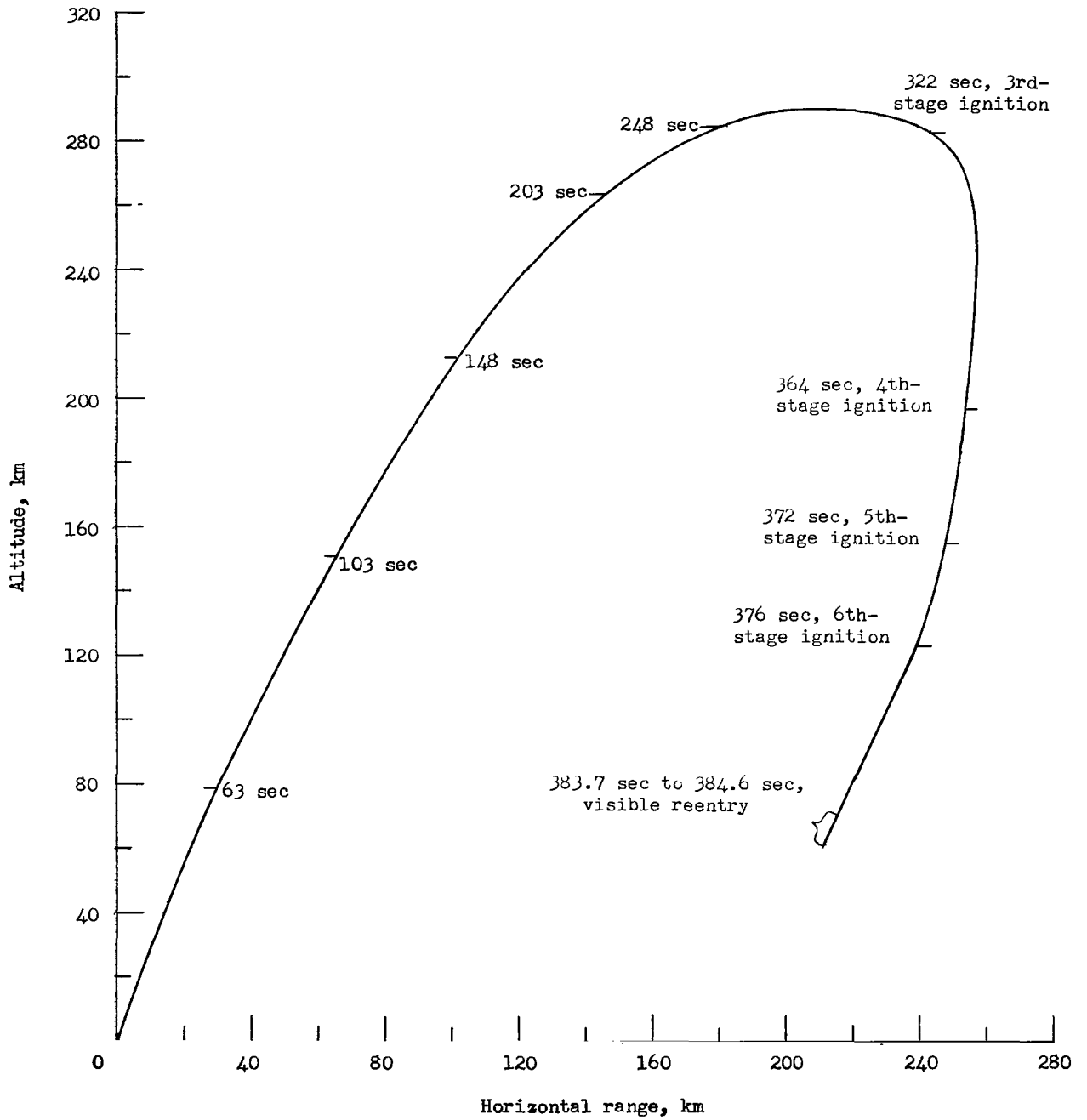


Figure 3.- Nominal trajectory of Trailblazer II vehicle.

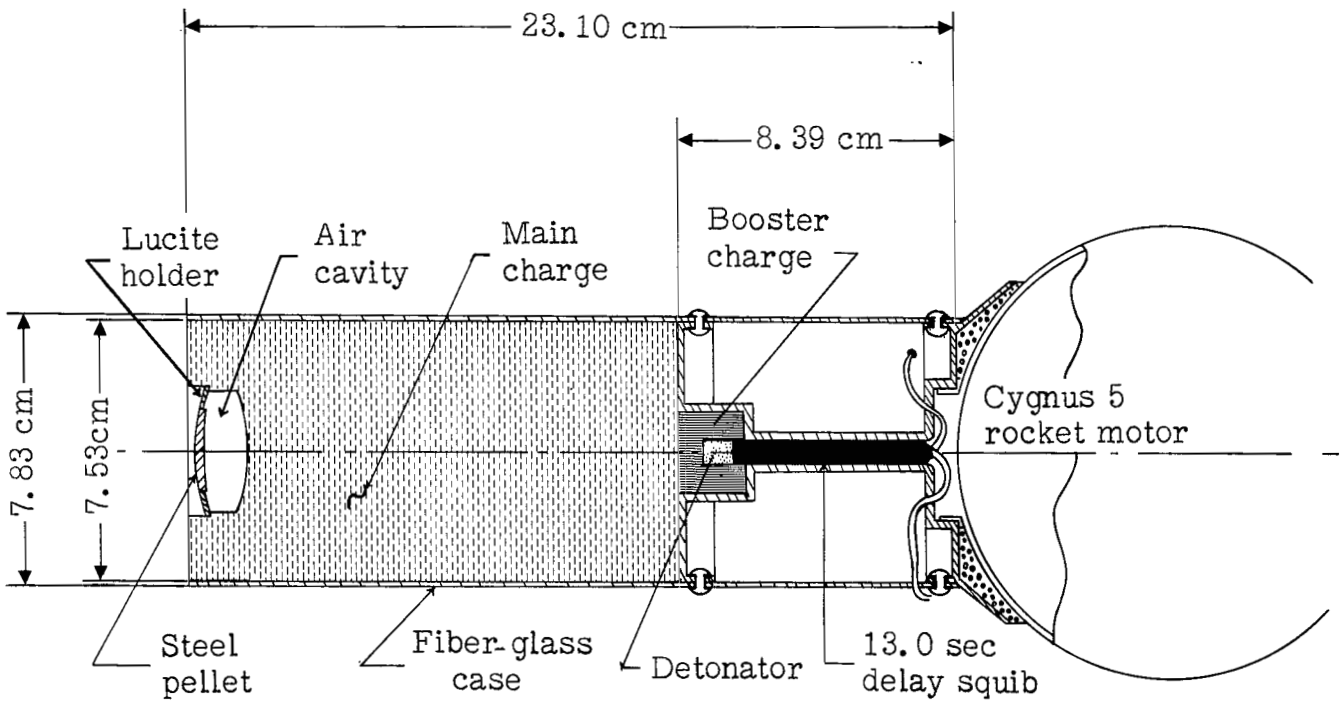


Figure 4.- Explosive accelerator (air cavity gun).

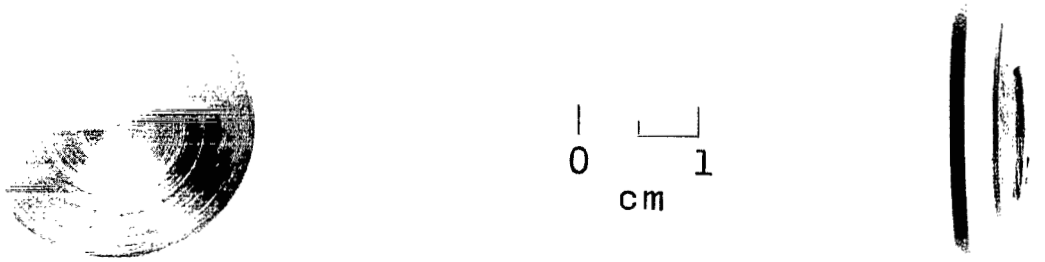


(a) Steel pellet and lucite retainer ring before ground test.

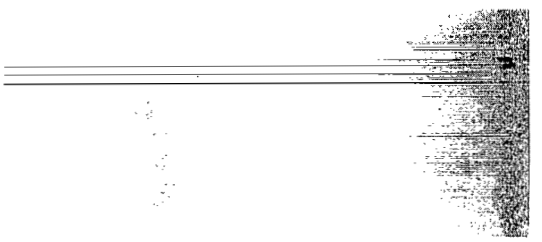

(b) Radiograph of main projectile and debris in flight during ground test.

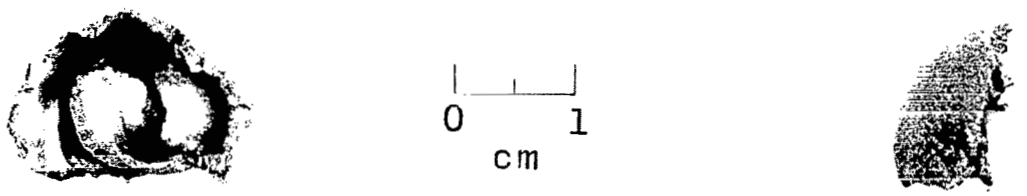


(c) Main projectile recovered from ground test. L-67-1099

Figure 5.- Composite photograph of results from ground test of type of air cavity gun used in artificial meteor experiment.

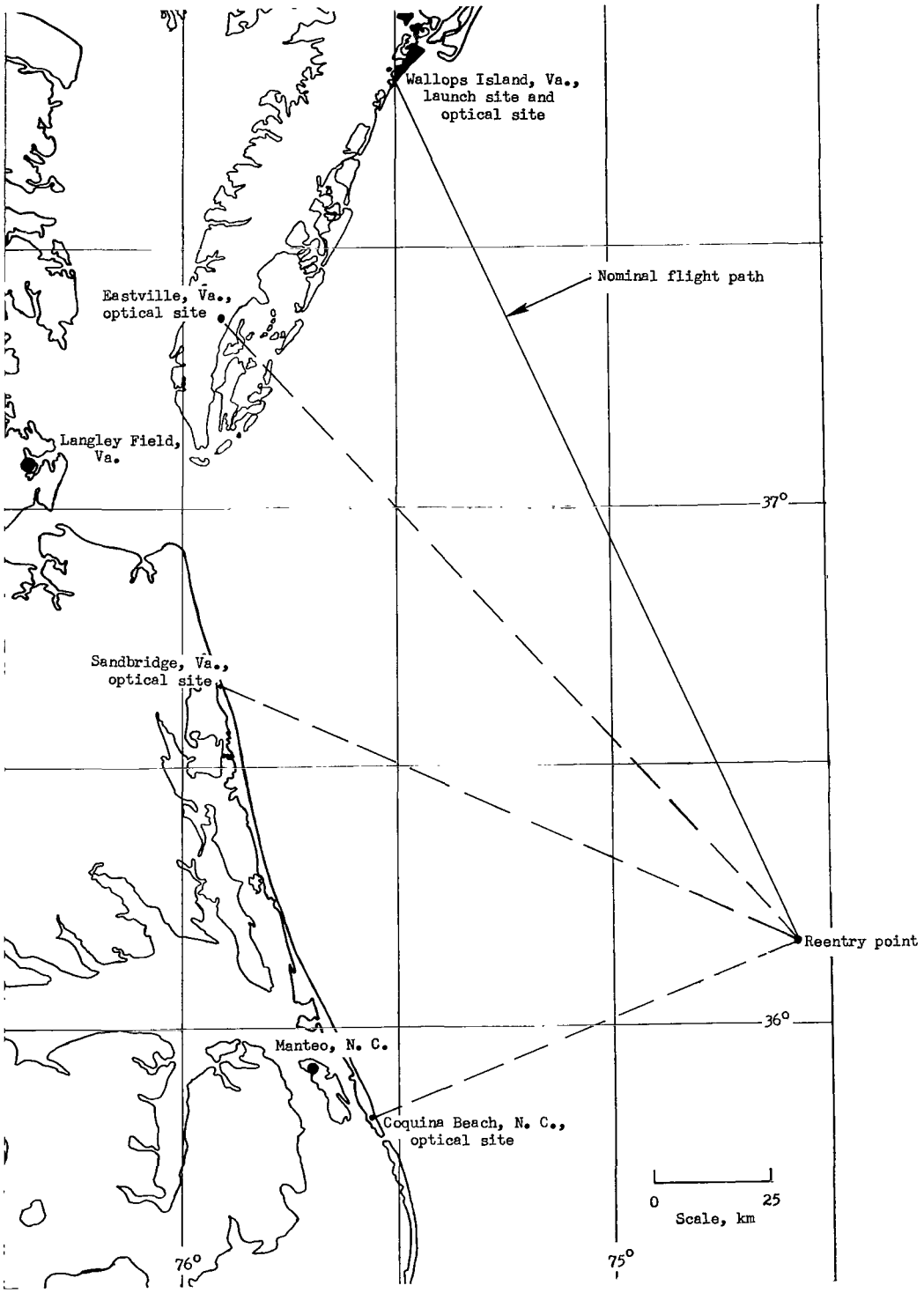


Figure 6.- Map of meteor simulation test range.

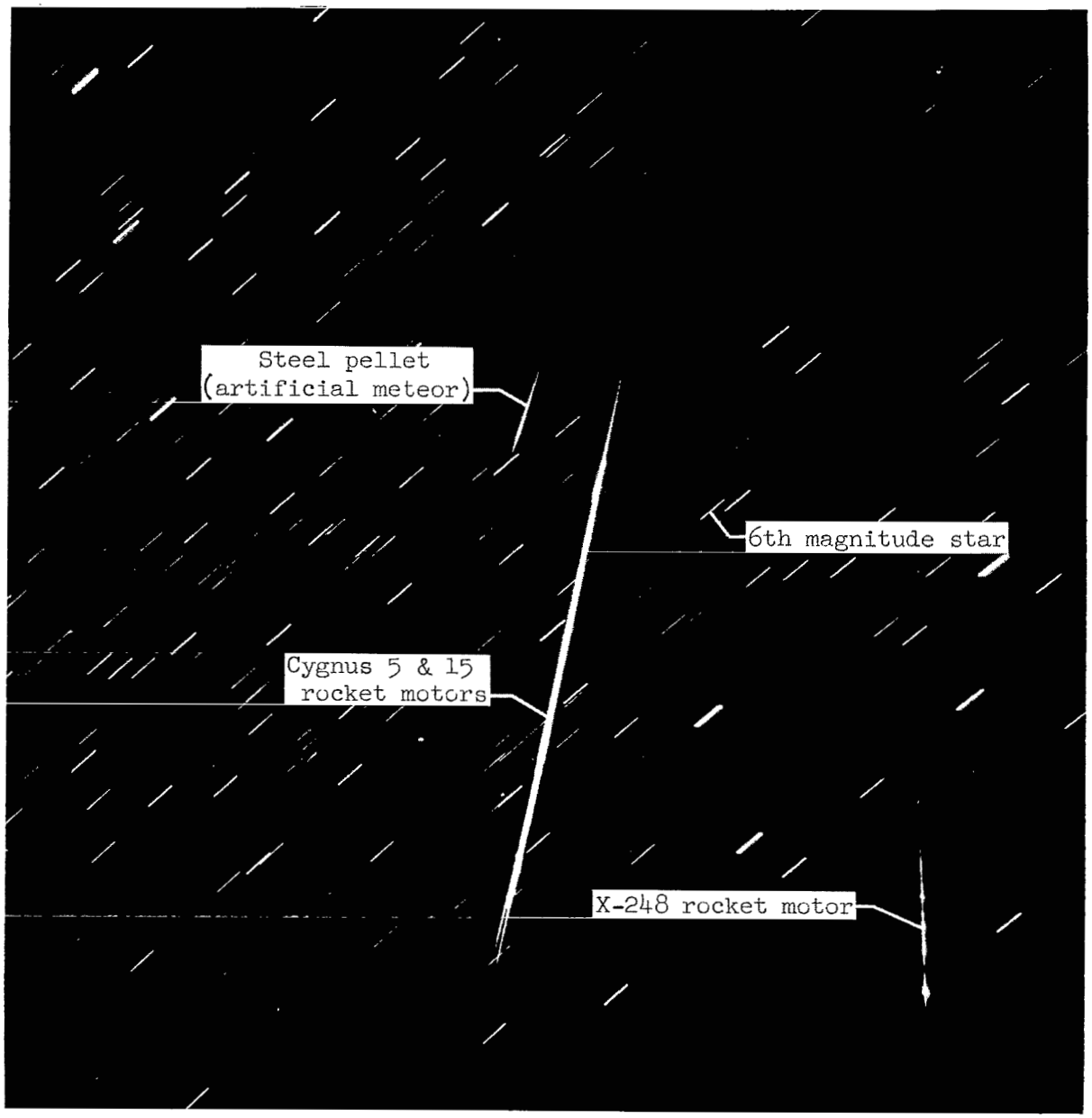


L-67-1098

Figure 7.- Photograph of meteor and rocket motor reentries taken from Sandbridge, Va., with BC-4 camera and blue sensitive film.

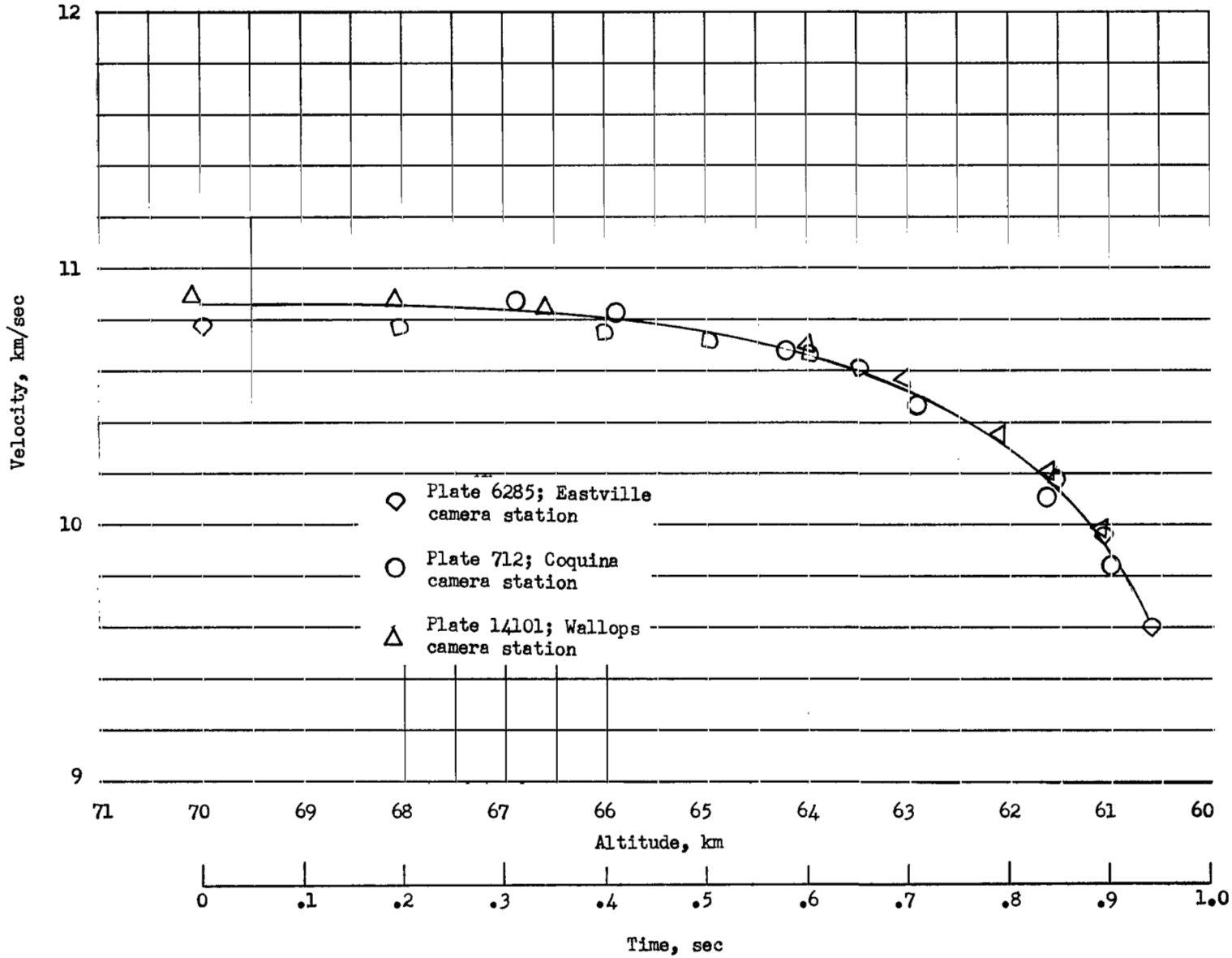


Figure 8.- Velocity of pellet plotted against altitude.

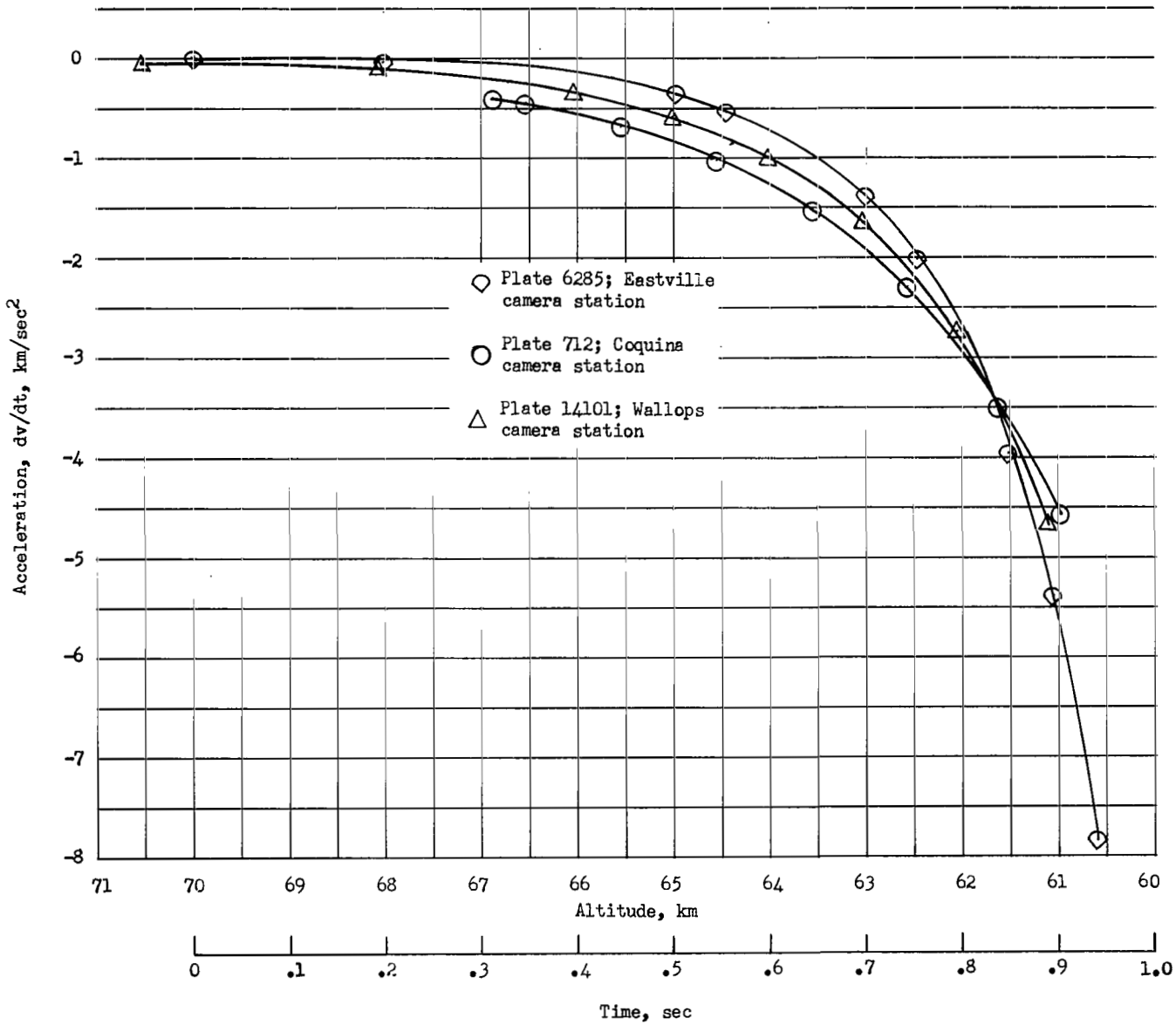


Figure 9.- Deceleration of pellet plotted against altitude.

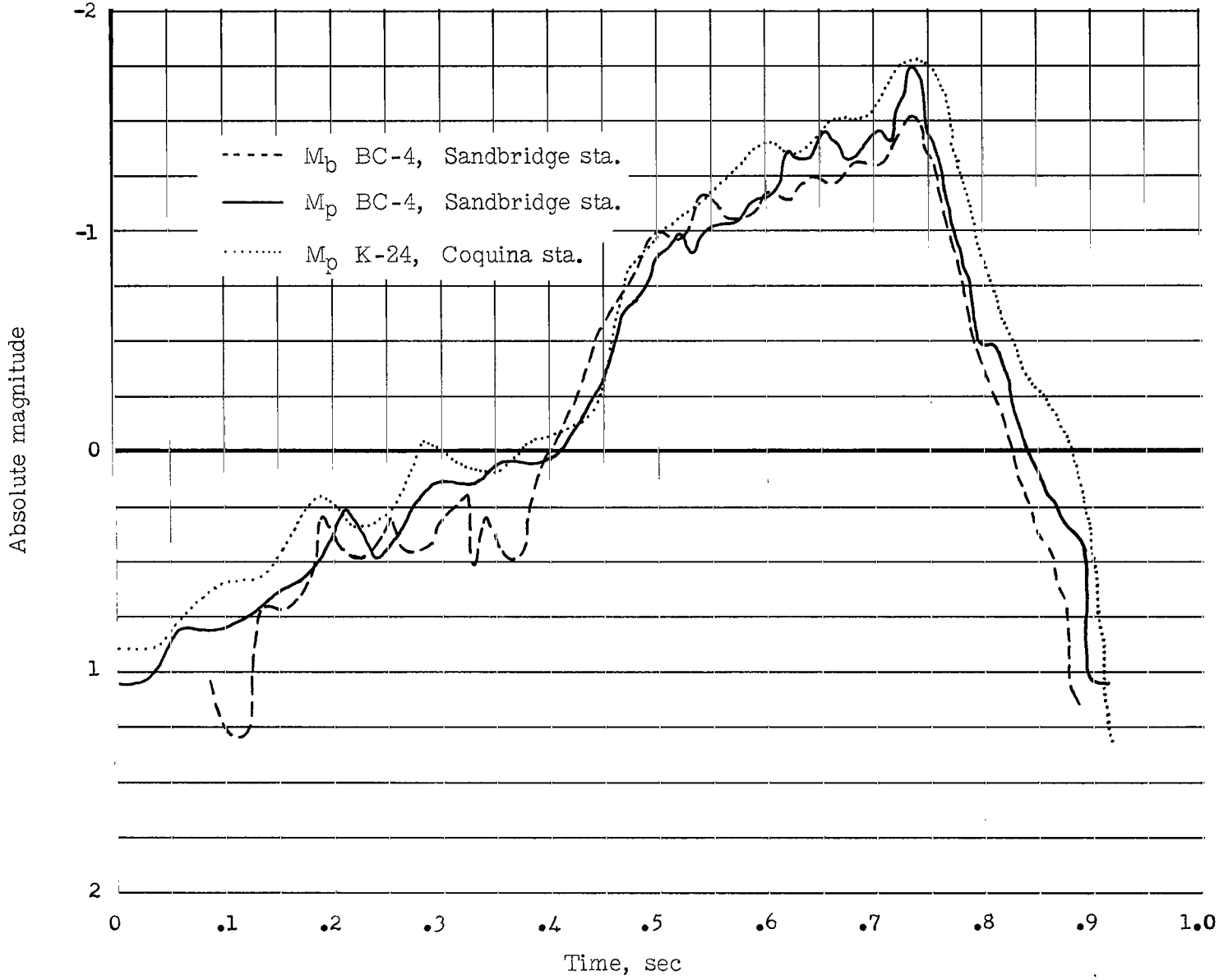


Figure 10.- Light curves of the meteor as determined from three photographic records.

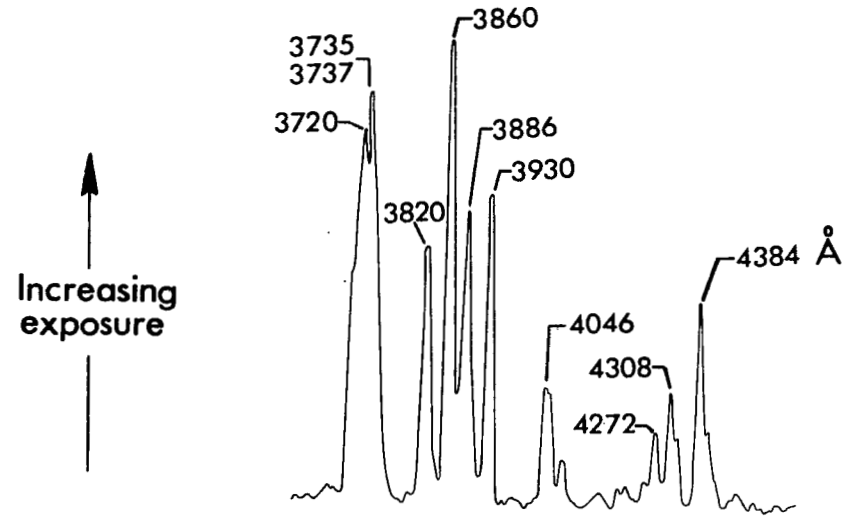


(a) Microphotometer trace of a prism spectrogram produced by a 5.7-gram iron artificial meteor at 10.8 km/sec. All refractive elements of the spectrograph were of standard optical glass.

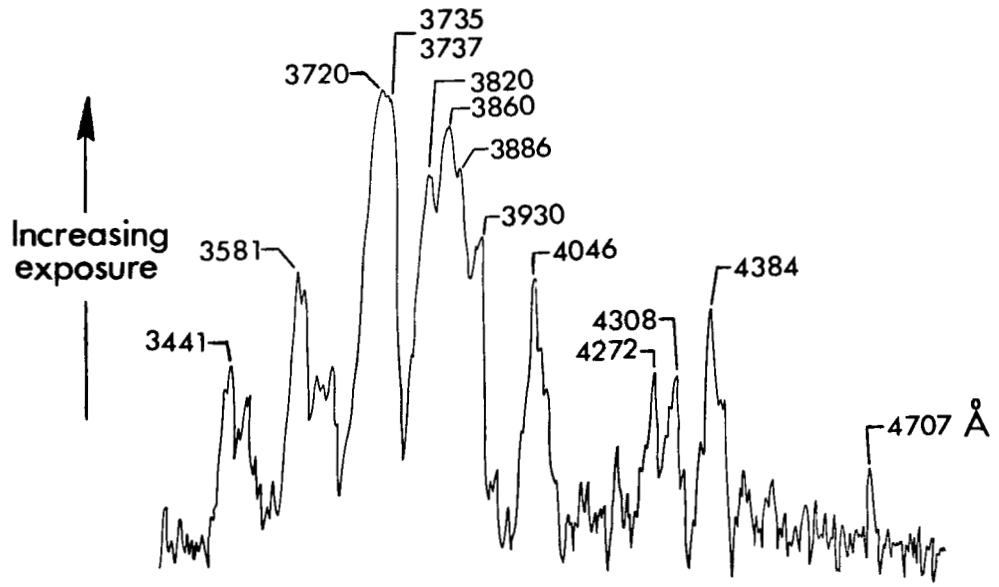


(b) Microphotometer trace of a grating spectrogram produced by a 0.6-gram iron artificial meteor at 9.5 km/sec. All refractive elements of the spectrograph were of fused silica.

Figure 11.- Comparison of the near ultraviolet spectrum of two artificial meteors.

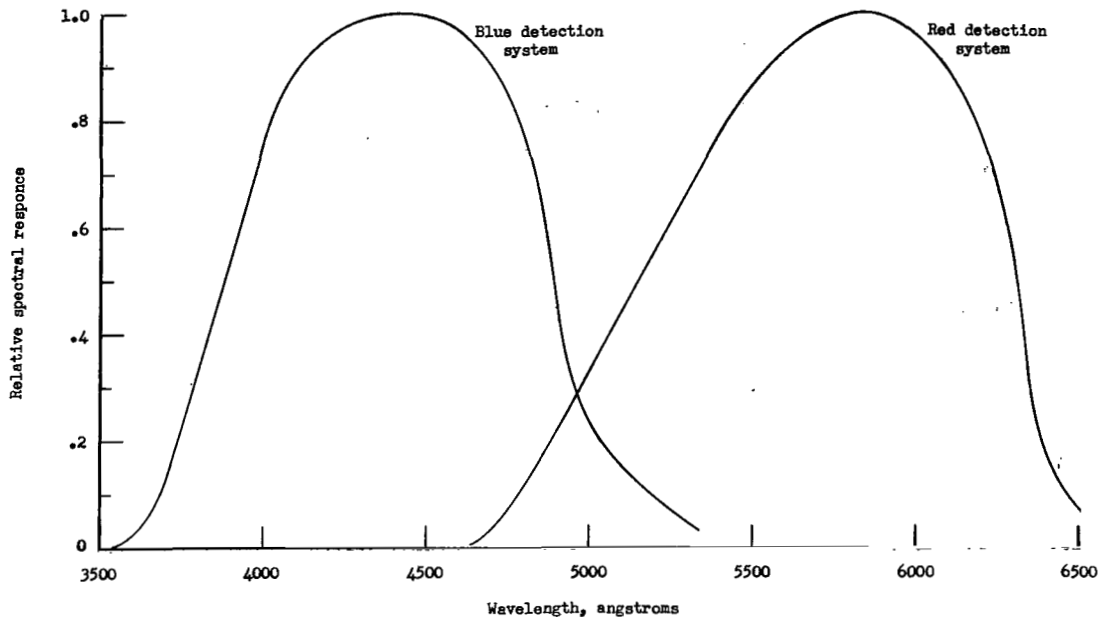


(a) Relative spectral response of two photographic detection systems.

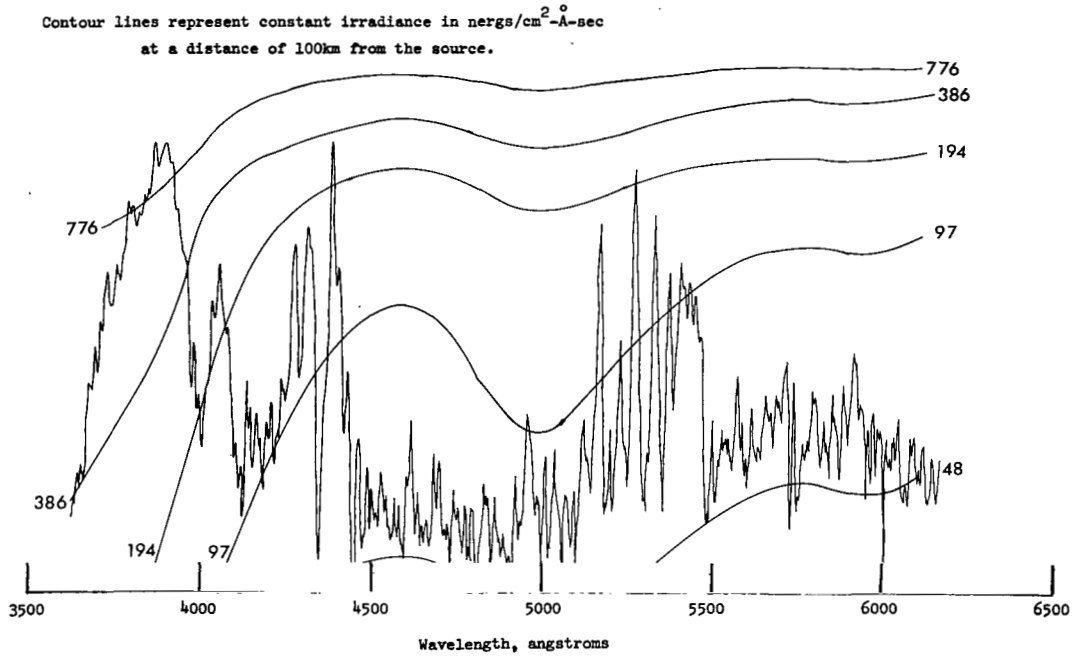


(b) Irradiance from an iron dust meteor. These data were taken from reference 9.

Figure 12.- Comparison of the spectral response of two broadband photographic detection systems to the spectra of an iron dust meteor.

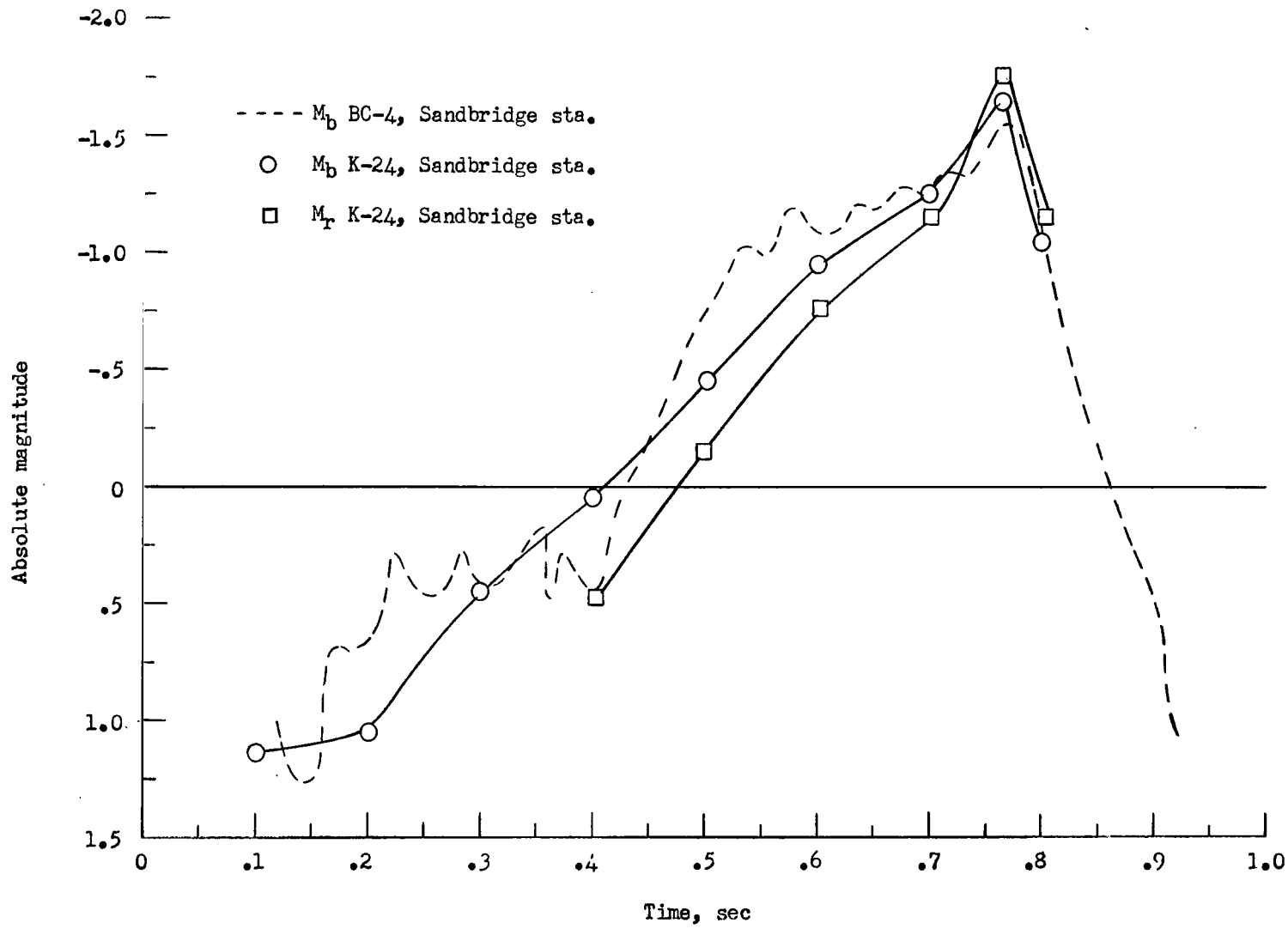


Figure 13.- Light curves for meteor in blue and red regions.

*"The aeronautical and space activities of the United States shall be conducted so as to contribute . . . to the expansion of human knowledge of phenomena in the atmosphere and space. The Administration shall provide for the widest practicable and appropriate dissemination of information concerning its activities and the results thereof."*

—NATIONAL AERONAUTICS AND SPACE ACT OF 1958

# NASA SCIENTIFIC AND TECHNICAL PUBLICATIONS

TECHNICAL REPORTS: Scientific and technical information considered important, complete, and a lasting contribution to existing knowledge.

TECHNICAL NOTES: Information less broad in scope but nevertheless of importance as a contribution to existing knowledge.

TECHNICAL MEMORANDUMS: Information receiving limited distribution because of preliminary data, security classification, or other reasons.

CONTRACTOR REPORTS: Scientific and technical information generated under a NASA contract or grant and considered an important contribution to existing knowledge.

TECHNICAL TRANSLATIONS: Information published in a foreign language considered to merit NASA distribution in English.

SPECIAL PUBLICATIONS: Information derived from or of value to NASA activities. Publications include conference proceedings, monographs, data compilations, handbooks, sourcebooks, and special bibliographies.

TECHNOLOGY UTILIZATION PUBLICATIONS: Information on technology used by NASA that may be of particular interest in commercial and other non-aerospace applications. Publications include Tech Briefs, Technology Utilization Reports and Notes, and Technology Surveys.

***Details on the availability of these publications may be obtained from:***

SCIENTIFIC AND TECHNICAL INFORMATION DIVISION

NATIONAL AERONAUTICS AND SPACE ADMINISTRATION

**Washington, D.C. 20546**